Electronic Supplementary Material (ESI) for Environmental Science: Processes & Impacts.

Supporting information for: Partitioning of reactive oxygen species from indoor surfaces to indoor aerosols

Glenn C. Morrison[1,*], Azin Eftekhari[2], Pascale S. J. Lakey[3], Manabu Shiraiwa[3], Bryan E. Cummings[4], Michael S. Waring[4], Brent Williams[5,6]

[1] Environmental Sciences and Engineering, Gillings School of Global Public Health, University of North Carolina at Chapel Hill, NC, USA

[2] Department of Chemical and Biomolecular Engineering, Georgia Institute of Technology, GA, USA

[3] Department of Chemistry, University of California Irvine, CA, USA

[4] Department of Civil, Architectural and Environmental Engineering, Drexel University, Philadelphia, PA, USA

[5]Department of Energy, Environmental and Chemical Engineering, Washington University in St. Louis, St. Louis, MO, USA

[6]Center for Aerosol Science and Engineering, Washington University in St. Louis, St. Louis, MO, USA

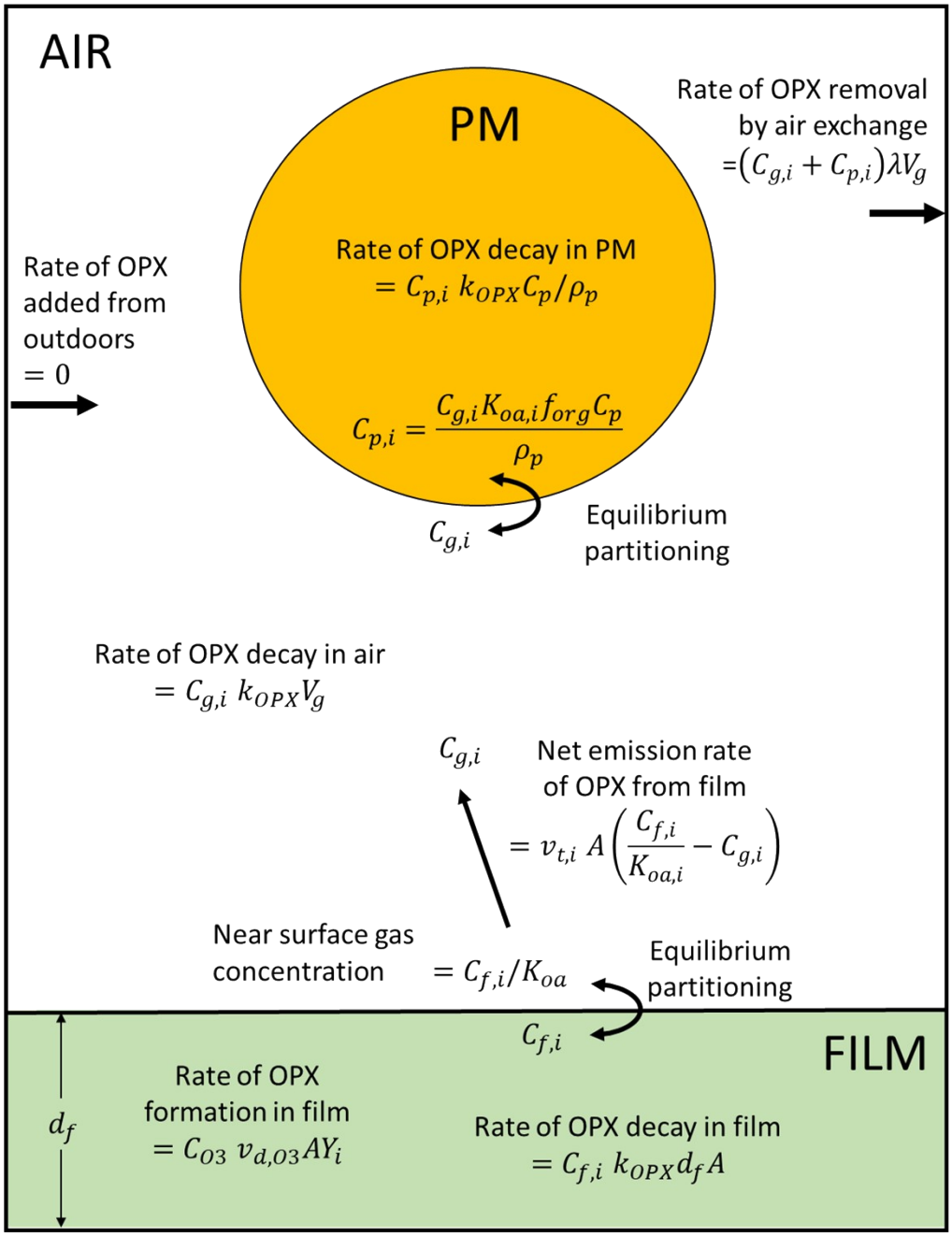

Figure S1. Diagram of main processes, with equations, implemented in model to find steady-state concentration of OPX in air, PM and film phases. Not shown are ozone or PM mass balance equations. See Table 1 and 2 for detailed description of variables.

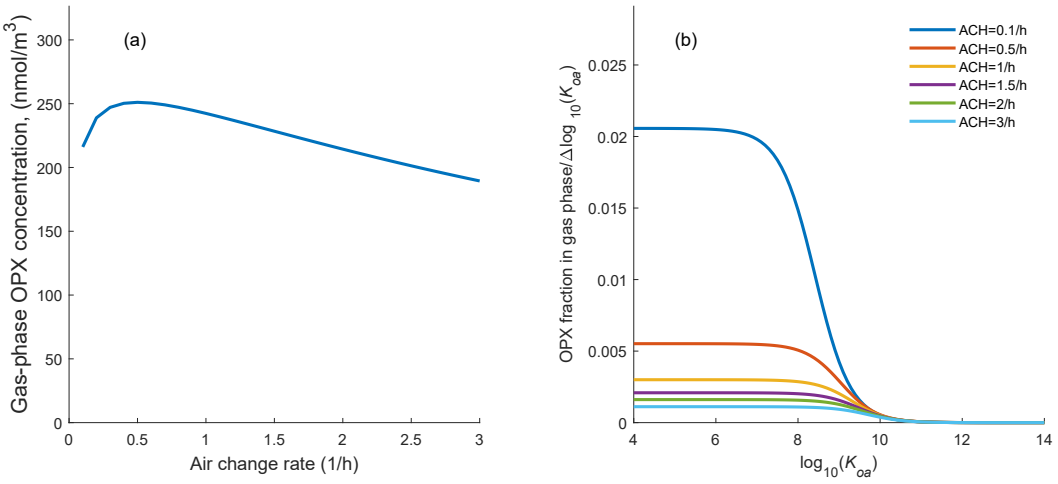

Figure S2. a) Gas-phase concentration of ROS as a function of air change rate for Case 1. b) fraction of species present in the gas as a function of $\log_{10}(K_{oa})$ for select air change rates (ACH). The majority of the gas-phase species have $\log_{10}(K_{oa})$ less than ~9.

Table S1. Products resulting from the reaction of palmitic acid with Criegee Intermediates formed from squalene ozonolysis. $Log_{10}(K_{oa})$ values are estimated from KOAWIN v1.10 in the Estimation Programs Interface (EPI) Suite. Also shown is one isomer of squalene hydroperoxide known to form in the reaction of ozone with skin lipids.[1,2]

Reaction	Product SMILES	$Log_{10}(K_{oa})$
palmitic acid + C3 CI from squalene ozonolysis	O=C(CCCCCCCCCCCCCCC)OC(C)(C)OO	11.8
palmitic acid + C8 CI from squalene ozonolysis	C(C)(C)=CCCC(C)(OC(=O)CCCCCCCCCCCCCCC)OO	13.4
palmitic acid + C13 CI from squalene ozonolysis	C(C)(C)=CCCC(C)=CCCC(C)(OC(=O)CCCCCCCCCCCCCCC)OO	15.1
palmitic acid + C17 CI from squalene ozonolysis	C(C)(C)=CCCC(C)=CCCC(C)=CCCC(OC(=O)CCCCCCCCCCCCCCC)OO	15.7
palmitic acid + C22 CI from squalene ozonolysis	C(C)(C)=CCCC(C)=CCCC(C)=CCCC=C(C)CCC(OC(=O)CCCCCCCCCCCCCCC)OO	17.4
palmitic acid + C27 CI from squalene ozonolysis	C(C)(C)=CCCC(C)=CCCC(C)=CCCC=C(C)CCC=C(C)CCC(OC(=O)CCCCCCCCCCCCCCC)OO	19.1
squalene hydroperoxide isomer	C(OO)(CCCC=C(CCC=C(CCC=C(C)C)C)C)(CCC=C(CCC=C(C)C)C)C	12.8

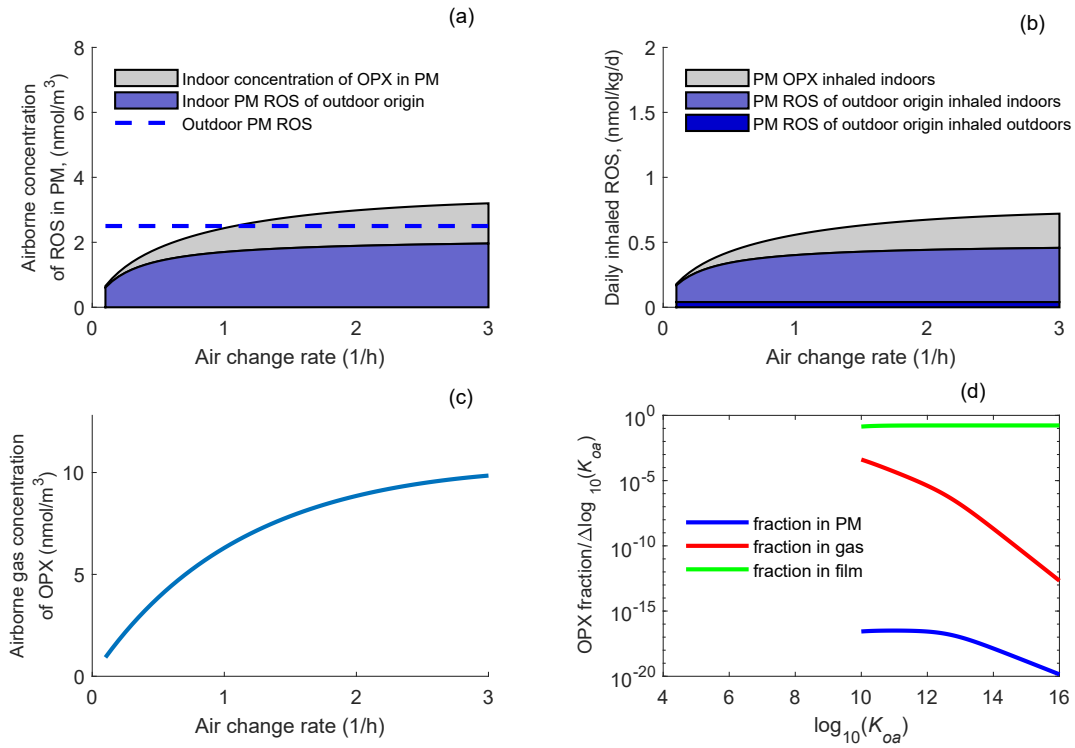

Figure S3. Case 1 simulation such that $\log_{10}K_{oa}$ ranges from 10 to 16, the gas-phase concentration (subplot (c)) of OPX is about 5 nmol/m^3 (0.3 ppb). Since more of the species formed are of lower volatility and produced with the same overall yield, they still increase the PM ROS substantially (subplot (a), 30% of ROS on PM that is of indoor origin for Case 1 for an air change rate of 1/h and with $10<K_{oa}<16$). Most of the OPX formed remains in the surface film: subplot (d) represents the OPX fraction in each phase, normalized by the width of the $\log_{10}(K_{oa})$ range.

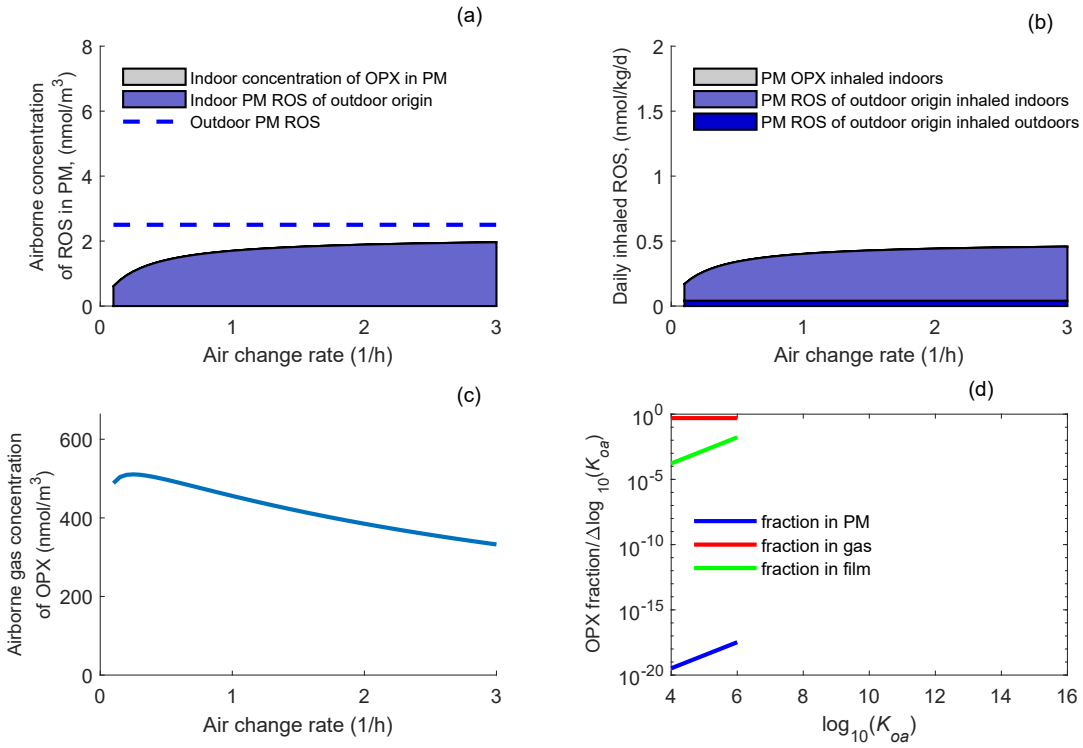

Figure S4. Case 1 simulation such that $\log_{10}(K_{oa})$ ranges from 4 to 6. Airborne concentration (a) and daily inhaled dose (b) of PM ROS of indoor origin is negligible. Most of the ROS is airborne (d), with a gas phase concentration of 400-500 nmol/m^3 (c). Subplot (d) represents the OPX fraction in each phase, normalized by the width of the $\log_{10}(K_{oa})$ range.

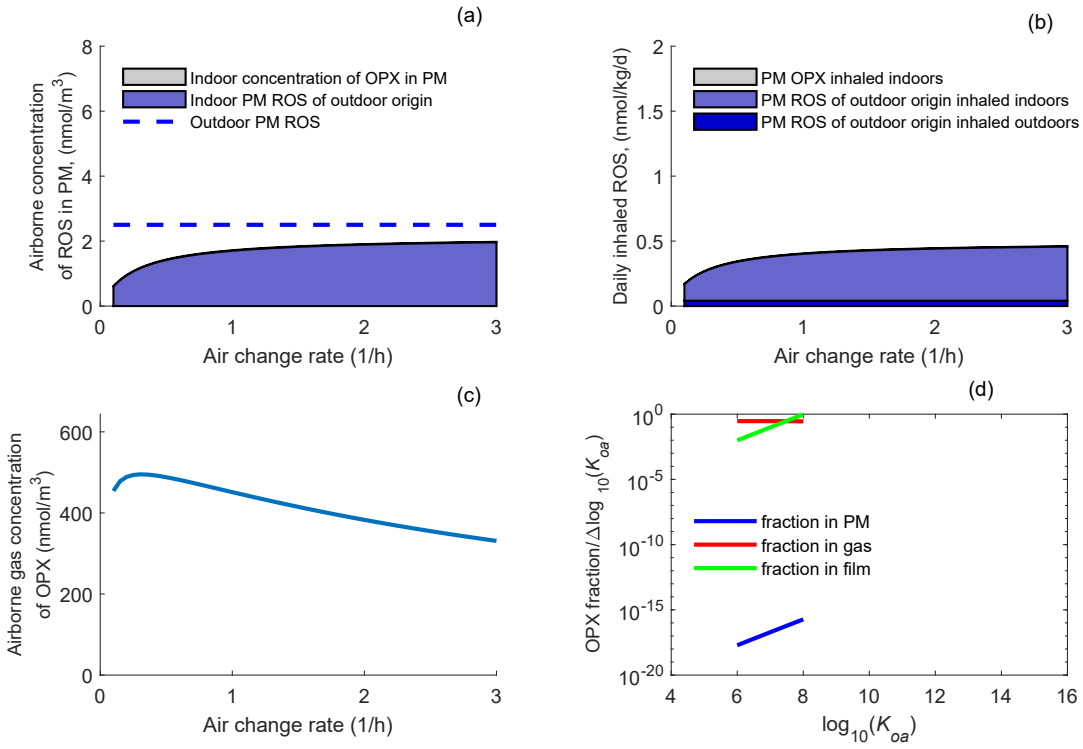

Figure S5. Case 1 simulation such that $\log_{10}(K_{oa})$ ranges from 6 to 8. Airborne concentration (a) and daily inhaled dose (b) of PM ROS of indoor origin is negligible. Most of the ROS is airborne (d), with a gas phase concentration of 400-500 nmol/m^3 (c). Subplot (d) represents the OPX fraction in each phase, normalized by the width of the $\log_{10}(K_{oa})$ range.

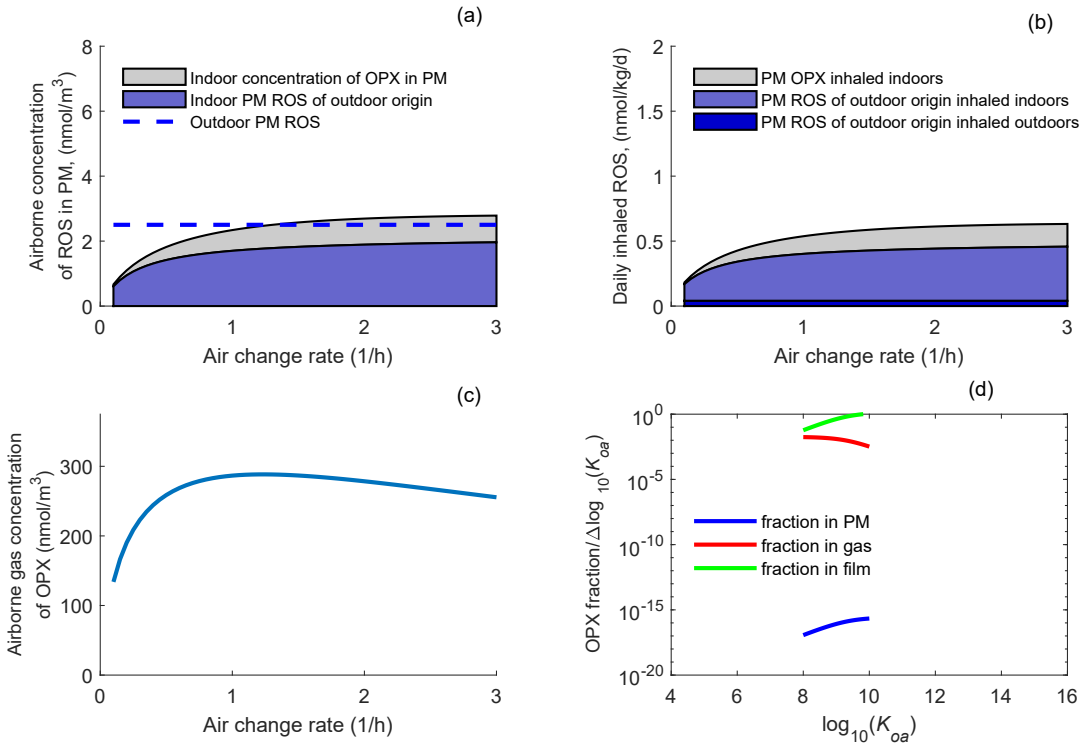

Figure S6. Case 1 simulation such that $\log_{10}(K_{oa})$ ranges from 8 to 10. Airborne concentration (a) and daily inhaled dose (b) of PM ROS of indoor origin is non-negligible. Most of the ROS is in the surface film (d), but the gas phase concentration of 150-300 nmol/m^3 (c) is relatively high. Subplot (d) represents the OPX fraction in each phase, normalized by the width of the $\log_{10}(K_{oa})$ range.

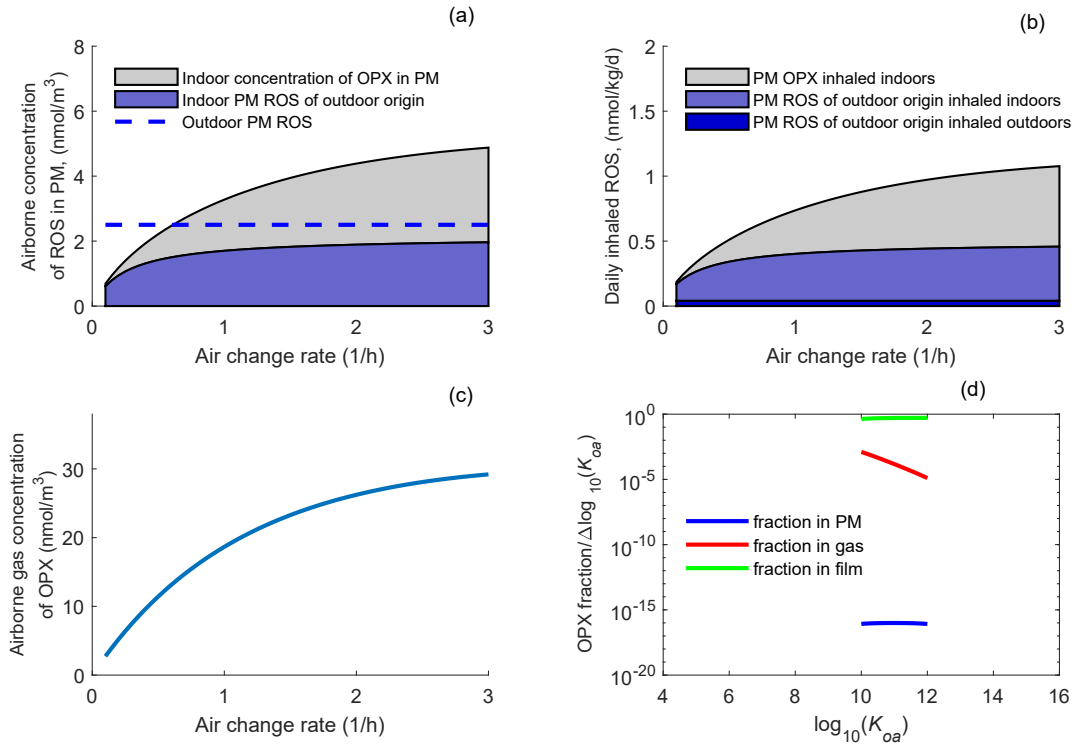

Figure S7. Case 1 simulation such that $\log_{10}(K_{oa})$ ranges from 10 to 12. Airborne concentration (a) and daily inhaled dose (b) of PM ROS of indoor origin is substantial relative to PM ROS of outdoor origin. Most of the ROS is in the surface film (d). Subplot (d) represents the OPX fraction in each phase, normalized by the width of the $\log_{10}(K_{oa})$ range.

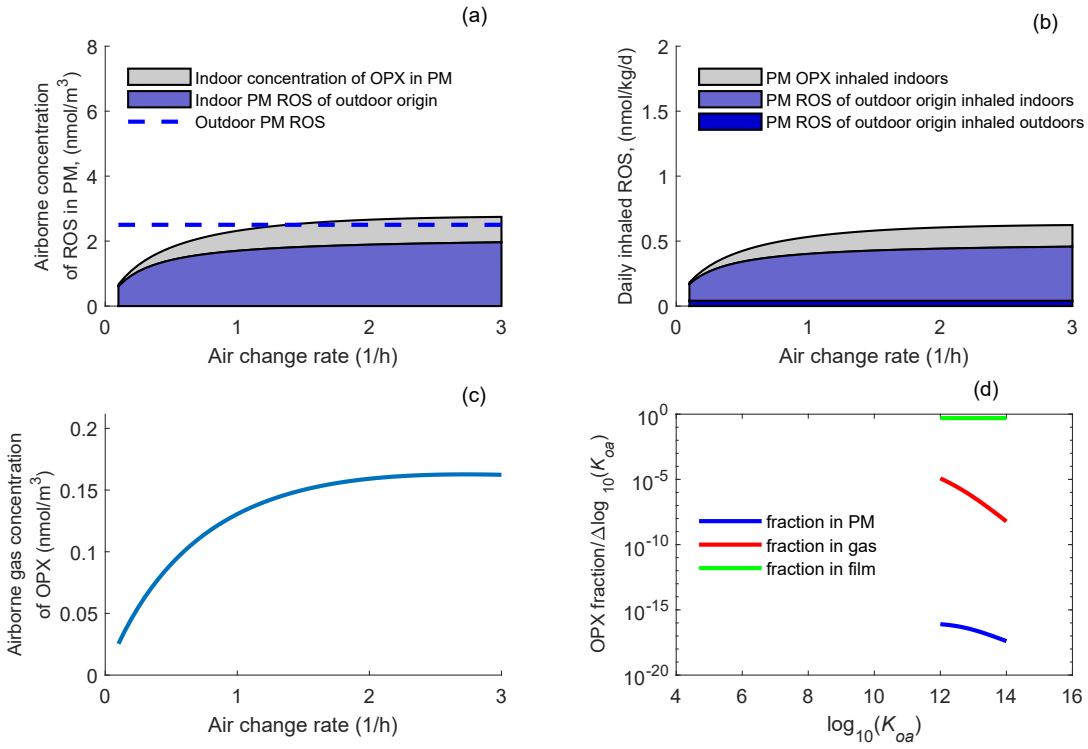

Figure S8. Case 1 simulation such that $\log_{10}(K_{oa})$ ranges from 12 to 14. Airborne concentration (a) and daily inhaled dose (b) of PM ROS of indoor origin is non-negligible relative to PM ROS of outdoor origin. Most of the ROS is in the surface film (d) and the gas-phase concentration is much lower than for simulations including lower ranges of K_{oa} (Figures S3-S6). Subplot (d) represents the OPX fraction in each phase, normalized by the width of the $\log_{10}(K_{oa})$ range.

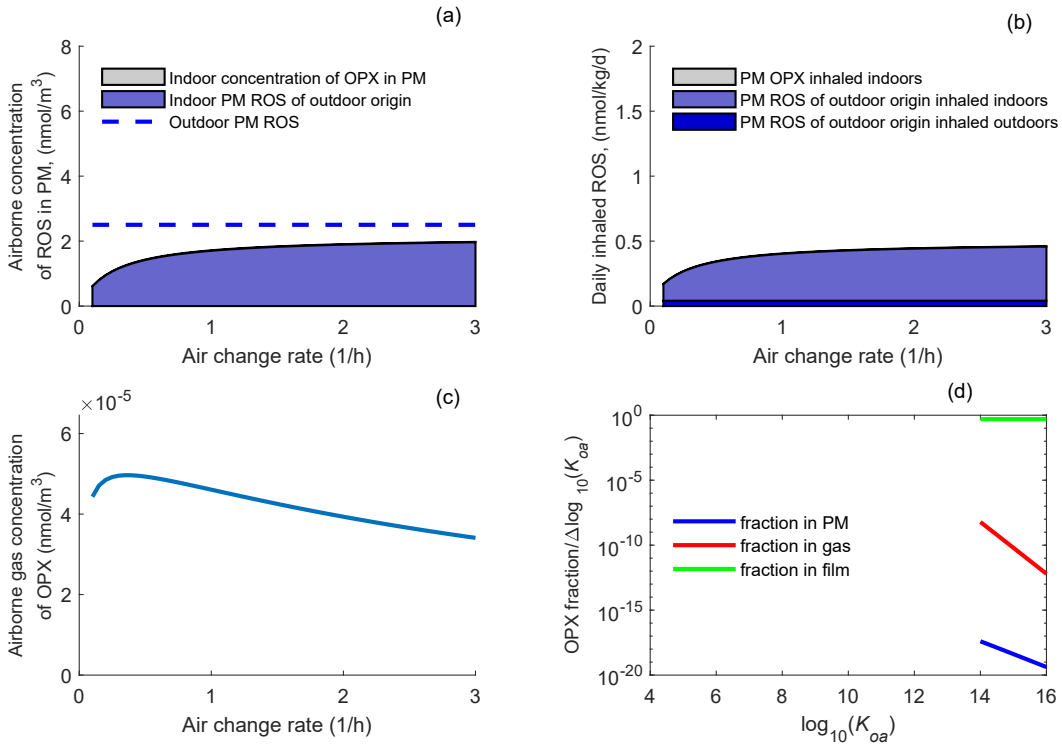

Figure S9. Case 1 simulation such that $\log_{10}(K_{oa})$ ranges from 14 to 16. Airborne concentration (a) and daily inhaled dose (b) of PM ROS of indoor origin is negligible relative to PM ROS of outdoor origin. Most of the ROS is in the surface film (d) and the gas-phase concentration is much lower than for simulations including lower ranges of K_{oa} (Figures S3-S7). Subplot (d) represents the OPX fraction in each phase, normalized by the width of the $\log_{10}(K_{oa})$ range.

S1. Influence of net surface sinks

The current model does not include sinks of OPX other than removal by decay or ventilation. It is possible that deposition to some surfaces, or transport into porous materials, could act as substantial additional sinks. Because it is not yet clear how these sinks should be included in the model, we estimate in a simple fashion the effect of a net surface sink on the resulting gas-phase concentration of OPX.

In the model, we assume all ozone-accessible surface area is coated uniformly in a reactive film. Instead, let 1/3 of the surface area be unreactive and act as a net and perfect sink of OPX. By reducing the surface area that is reactive by 2/3, we reduce the rate of OPX generation by 2/3. The unreactive surface area now acts as a sink that can be related to the air exchange rate (the major sink when the air exchange rate is around 1/h). The equivalent surface sink rate is

$$\left(\frac{1}{3}\right)\left(\frac{A}{V}\right)v_{t,i} = \left(\frac{1}{3}\right)(3/m) * 3\frac{m}{h} = 3/h$$

In the simulation, the gas-phase concentration of OPX was about 240 nmol/m^3 for Case 1 at 1 air change per hour. An estimate of the influence of the net surface sink described above is

$$C_{g,with\ sink} = (240\frac{nmol}{m^3})\left(\frac{2}{3}\right)\left(\frac{1/h}{1/h + 3/h}\right) = 40\frac{nmol}{m^3}$$

The gas-phase concentration of OPX is reduced by a factor of 6. The PM OPX would also be reduced by a factor of six.

This scenario assumes that removal by deposition occurs at the transport-limited rate (due to the surface being a perfect sink) and may overestimate the reduction in OPX gas-phase concentrations.

References

(1) Shimizu, N.; Bersabe, H.; Ito, J.; Kato, S.; Towada, R.; Eitsuka, T.; Kuwahara, S.; Miyazawa, T.; Nakagawa, K. Mass Spectrometric Discrimination of Squalene Monohydroperoxide Isomers. *Journal of Oleo Science* **2017**, *66* (3), 227–234. https://doi.org/10.5650/jos.ess16159.

(2) Curpen, S.; Francois-Newton, V.; Moga, A.; Hosenally, M.; Petkar, G.; Soobramaney, V.; Ruchaia, B.; Lutchmanen Kolanthan, V.; Roheemun, N.; Sokeechand, B. N.; Aumeeruddy, Z.; Ramracheya, R. D. A Novel Method for Evaluating the Effect of Pollution on the Human Skin under Controlled Conditions. *Skin Research and Technology* **2020**, *26* (1), 50–60. https://doi.org/10.1111/srt.12763.